entropy, although the difference has been substantially reduced. Smooth extrapolation of C_p (liquid) below T_g and of the corresponding entropy indicate the existence of a positive "Kauzmann temperature" T_K at which the crystal and the extrapolated liquid attain equal entropies (*19*). Considering that vibrational entropies are nearly the same for the two phases, and that the inherent structural entropy of the ordered crystal vanishes, the fully relaxed glass at T_K (the extrapolated liquid) must also have vanishing inherent structural entropy. This realization, coupled with the empirical observation that $T_K \cong T_0$, the mean relaxation-time divergence temperature, has generated the concept of an "ideal glass state" that could be experimentally attained if only sufficiently slow cooling rates were available (*20*).

If indeed it exists, the ideal glass state must correspond to the inherent structure with the lowest potential energy (deepest "crater") that is devoid of substantial regions with local crystalline order. Unfortunately, the details of this noncrystallinity constraint are unclear but may be crucial: Qualifying inherent structures may depend on the maximum size and degree of perfection permitted crystalline inclusions in otherwise amorphous structures. This ambiguity, or non-uniqueness of choice criterion, would seem to undermine the concept of a substantially unique ideal glass state.

It has also been argued (*9*) that the seemingly innocuous extrapolations that identify a positive Kauzmann temperature T_K (and by implication T_0) are flawed. Localized particle rearrangements (associated with β relaxations) are always possible, even in a hypothetical ideal glass structure, and raise the potential energy only by O(1). These structural excitations in the strict sense prevent attaining the ideal glass state at positive temperature, in conflict with the usual view (*20*).

In spite of these formal reservations, the ideal glass state concept remains valuable. Careful and systematic experiments on the most fragile glass formers should help to remove some of the obscuring uncertainties.

Conclusions

By focusing attention on the topographic characteristics of Φ in the multidimensional configuration space, a comprehensive description becomes available for static and kinetic phenomena exhibited by supercooled liquids and their glass transitions. In particular, this viewpoint rationalizes the characteristic properties of fragile glass formers, including non-Arrhenius viscosity, primary-secondary relaxation bifurcation, and the enhancement of self-diffusion rates over the Stokes-Einstein prediction. This multidimensional topographic representation has the further benefit of uncovering and promoting several basic research topics that need sustained experimental and theoretical-simulational attention. Examples of the latter are the material-specific enumeration of inherent structures (Φ minima), the exploitation of the Lindemann-like freezing criterion for liquids and its relation to the glass transition, and the critical evaluation of the ideal-glass-state concept.

REFERENCES AND NOTES

1. J. D. Bernal, *Nature* **183**, 141 (1959); H. Eyring *et al.*, *Proc. Natl. Acad. Sci. U.S.A.* **44**, 683 (1958); M. R. Hoare, *Adv. Chem. Phys.* **40**, 49 (1979).
2. M. Goldstein, *J. Chem. Phys.* **51**, 3728 (1969); *ibid.* **67**, 2246 (1977).
3. For constant-pressure circumstances, system volume becomes an additional coordinate and Φ includes a pressure-volume contribution *PV*.
4. F. H. Stillinger and T. A. Weber, *Science* **225**, 983 (1984).
5. ———, *Phys. Rev. A* **25**, 978 (1982).
6. F. A. Lindemann, *Z. Phys.* **11**, 609 (1910).
7. H. Löwen, *Phys. Rep.* **237**, 249 (1994).
8. R. A. LaViolette and F. H. Stillinger, *J. Chem. Phys.* **83**, 4079 (1985).
9. F. H. Stillinger, *ibid.* **88**, 7818 (1988).
10. G. W. Scherer, *J. Am. Ceram. Soc.* **75**, 1060 (1992).
11. K. L. Ngai, Comments *Solid State Phys.* **9**, 127 and 141 (1979); R. Böhmer, K. L. Ngai, C. A. Angell, D. J. Plazek, *J. Chem. Phys.* **99**, 4201 (1993).
12. E. W. Montroll and J. T. Bendler, *J. Stat. Phys.* **34**, 129 (1984).
13. G. P. Johari and M. Goldstein, *J. Chem. Phys.* **53**, 2372 (1970).
14. F. H. Stillinger, *Phys. Rev. B* **41**, 2409 (1990).
15. C. A. Angell, in *Relaxations in Complex Systems*, K. Ngai and G. B. Wright, Eds. (National Technical Information Service, U.S. Department of Commerce, Springfield, VA, 1985), p. 1.
16. F. Fujara, B. Geil, H. Sillescu, G. Fleischer, *Z. Phys. B* **88**, 195 (1992); M. T. Cicerone and M. D. Ediger, *J. Phys. Chem.* **97**, 10489 (1993); R. Kind *et al.*, *Phys. Rev. B* **45**, 7697 (1992).
17. M. T. Cicerone, F. R. Blackburn, M. D. Ediger, *J. Chem. Phys.* **102**, 471 (1995).
18. F. H. Stillinger and J. A. Hodgdon, *Phys. Rev. E* **50**, 2064 (1994).
19. W. Kauzmann, *Chem. Rev.* **43**, 219 (1948).
20. J. Jäckle, *Rep. Prog. Phys.* **49**, 171 (1986).

The Microscopic Basis of the Glass Transition in Polymers from Neutron Scattering Studies

B. Frick* and D. Richter

Recent neutron scattering experiments on the microscopic dynamics of polymers below and above the glass transition temperature T_g are reviewed. The results presented cover different dynamic processes appearing in glasses: local motions, vibrations, and different relaxation processes such as α- and β-relaxation. For the α-relaxation, which occurs above T_g, it is possible to extend the time-temperature superposition principle, which is valid for polymers on a macroscopic scale, to the microscopic time scale. However, this principle is not applicable for temperatures approaching T_g. Below T_g, an inelastic excitation at a frequency of some hundred gigahertz (on the order of several wave numbers), the "boson peak," survives from a quasi-elastic overdamped scattering law at high temperatures. The connection between this boson peak and the fast dynamic process appearing near T_g is discussed.

Polymers have a very wide range of applicability and can be used in the solid, rubbery, or molten states. Solid polymers are used whenever elastic strength is required, and melts are used whenever viscous properties are desired. The intermediate range of viscoelasticity has particularly interesting properties and covers an especially wide temperature range for polymers because of their chain structure. Ideally, an understanding of the microscopic dynamics would be a prerequisite for optimized application. The limiting cases of the elastic solid and the viscous liquid are better understood than the viscoelastic regime, although a large amount of experimental data exists for the viscoelastic state (*1*). Polymers are generally amorphous solids, that is, they are microscopically disordered without translational symmetry and crystallization is rare. The microscopic disorder remains essentially unchanged as the polymer transforms from the glassy solid state to the melt or liquid state (Fig. 1A).

The key to understanding the property changes is the change of the microscopic dynamics, and any structural changes are therefore a consequence of it. Microscopically, elastic solids are characterized by their atoms or molecules being bound within a potential defined by the surrounding atoms.

B. Frick is in the Institut Laue-Langevin, BP156, F-38042 Grenoble Cedex 9, France. D. Richter is in the Institut für Festkörperforschung, Forschungsanlage Jülich, D-52425 Jülich, Germany.

*To whom correspondence should be addressed.

The restoring force within the potential is determined by the elastic constant K. The particles undergo vibrations, librations, or rotations around their rest positions in the potential minima and also show collective excitations (that is, phonons) at lower energies. In contrast, the viscous state is characterized by delocalized atoms or molecules that translate and diffuse and experience during their motion a friction characterized by the friction constant ζ or the diffusion constant $D = k_B T/\zeta$, where k_B is the Boltzmann constant and T is the temperature. Collective excitations in the viscous state are usually strongly overdamped.

Unlike ordinary phase transitions, which occur at a well-defined temperature, the glass transition temperature T_g, which separates the elastic glassy state from the viscoelastic state, depends on the time scale of the experiment. It is usually defined in terms of the viscosity, which at T_g reaches a value of about 10^{13} poise, corresponding to structural or "α-relaxation" times of several hundred seconds. Indeed, the functional form that is commonly used to describe the shear viscosity η, the Vogel-Fulcher or Williams-Landel-Ferry law, does not diverge at

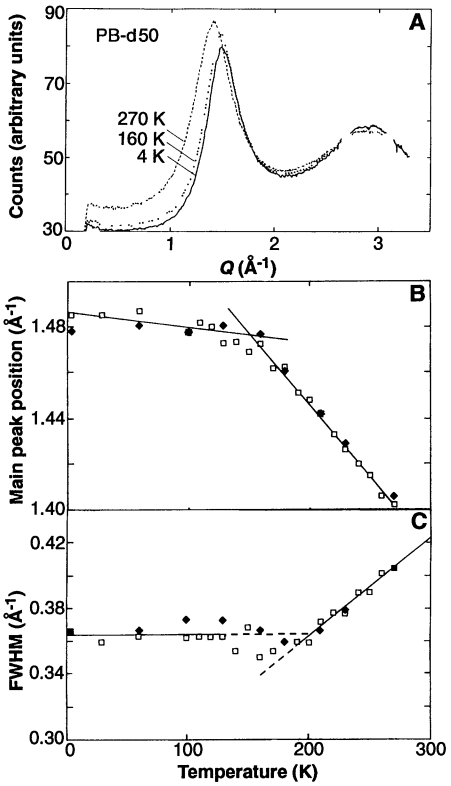

Fig. 1. Temperature dependence of (**A**) the static structure factor, (**B**) the main peak position, and (**C**) the line width of the main peak for fully deuterated polybutadiene [$T_g \sim 186$ K; microstructure: 47% cis (1.4) units, 46% trans (1.4) units, 7% vinyl (1.2) units] (*29*). Filled symbols, molecular weight $M_w = 50{,}000$; open symbols, $M_w = 95{,}000$. (A) is for $M_w = 50{,}000$.

T_g but at a temperature T_0 below T_g: $\eta = A\exp[C/(T - T_0)]$, where C and A are constants. This property led to speculation about an underlying phase transition below T_g at T_0 (*2*). There are, however, many arguments against this hypothesis (*3*).

A different type of transition, a dynamic phase transition, has been proposed by the mode coupling theory (MCT) to explain the origin of the glass transition (*4*). The detailed predictions of the MCT for the change of the microscopic dynamics has revitalized research into glasses and the glass transition. In MCT, a liquid is described by a Langevin equation for density correlation functions, including a memory term that is formulated in the mode-coupling approximation. Below a critical temperature T_c, relaxations in the liquid-like system are arrested, and spontaneous breaking of ergodicity occurs (that is, the system no longer explores the phase space uniformly). Above this critical temperature, according to the idealized MCT, the density relaxations take place in a two-step form, commencing with a so-called "fast β-relaxation" and continuing with the second step, the "structural α-relaxation," whereas below T_c only the fast β-relaxation persists. Later versions of MCT include hopping processes, which smear T_c and maintain the α-relaxation or transport even below the critical temperature T_c.

Dynamical Behavior of Polymer Glasses

Glass-forming systems in general and polymer systems in particular exhibit motional processes over an extremely broad range in time. The following features are noteworthy. (i) The structural or α-relaxation, which is connected to the viscous flow, is characterized by a Vogel-Fulcher temperature dependence and becomes extremely slow at T_g. (ii) At a temperature somewhat above T_g, an additional motional process in general separates from the α-process, which we call the Johari-Goldstein or "slow" β-process (*5*) and which is usually observed by dielectric measurements. From the merging temperature downward, the Johari-Goldstein process follows an Arrhenius behavior with a typical barrier height on the order of 10 to 20 $k_B T_g$. (iii) Most glass-forming systems exhibit in addition a fast process with a time constant in the picosecond range (that has at most a very weak dependence on temperature, as observed by neutron and Raman scattering). (iv) Below T_g, an additional vibrational density of states is found at low frequencies, which gives rise to the so-called "boson peak," a feature that appears to be connected with the low-temperature anomalies in glasses. (v) In addition to these general features, system-specific relaxations occur that are related to internal degrees of freedom, such as side-group motions. Before we briefly discuss the characteristics of these different dynamic processes as elucidated by neutron scattering techniques, we make some short comments on the latter.

Neutron Scattering Fundamentals

Neutrons offer the unique possibility of analyzing the spatial dimensions of atomic or molecular processes in their development over time, in contrast to electromagnetic waves, which either achieve atomistic space resolution through x-ray or synchrotron radiation or high temporal resolution through laser light pulses. Thus, x-rays show the location of an atom or a molecule, and optical spectroscopy yields information about molecular processes in terms of time without making statements on the location. Inelastic neutron scattering, however, answers the question of where an atom moves at what rate and to what place. It thus furnishes complete information about atomic and molecular processes. Nuclear magnetic resonance (NMR) and dielectric experiments are complementary in that they explore the dynamics on a longer time scale and less spatial information can be extracted. Second, because the neutron scattering cross section of atomic species depends on the isotope, individual atoms can be detected among atoms of the same species by isotope exchange without major chemical modifications. The highly different scattering of heavy and light hydrogen is particularly useful in this regard. Individual organic molecules such as polymers can thus be made visible or can be "decorated" among species of the same type by partial deuteration. This feature is often applied in the study of the dynamics and structure of organic materials and has, just to cite one early example, led to the clarification of the bulk polymer conformation (*6*). Here we show how these properties can be used to study the local dynamics and structure of polymers in the glass transition range.

In a neutron scattering experiment, neutrons enter a sample with defined momentum and defined energy, are scattered by the atomic nuclei, and leave the sample with changed momentum and changed energy. The momentum transfer $\hbar\mathbf{Q} = \hbar\mathbf{K}_0 - \hbar\mathbf{K}$, where $\mathbf{K}_0$ and $\mathbf{K}$ are the momentum of the neutron before and after the scattering event and $\hbar$ is Planck's constant h divided by 2π, contains information about the spatial distance, which is important for the scattering process: Spatial distance and momentum are inversely proportional. The energy change $\hbar\omega = [\hbar^2/2m_n](|\mathbf{K}_0|^2 - |\mathbf{K}|^2)$, where m_n is neutron mass and ω is the reduced frequency, provides information about the associated time scale of motion: The time t and the energy $\hbar\omega$ also show inverse behavior.

In general, the scattering function $S(\mathbf{Q}, \omega)$ is measured. It describes the probability with which a neutron can transfer the corresponding energy and momentum to the sample and thus contains information about the sample structure and dynamics. By the so-called van Hove formalism, $S(\mathbf{Q}, \omega)$ is linked to the pair correlation function $G(\mathbf{R}, t)$ by Fourier transformation. It describes the probability of finding two atoms at the location $\mathbf{R}$ in the time interval t. For the special case of incoherent scattering (*7*), the scattering function $S_{inc}(\mathbf{Q}, \omega)$ is related to the self-correlation function $G_s(\mathbf{R}, t)$, which describes the probability of finding the same atom after a time interval t at the location $\mathbf{R}$. Concerning the information content of such scattering functions, we can consider, for example, the incoherent scattering function from a vibrating system. In this case, $S_{inc}(|\mathbf{Q}|, \omega)$ measures the effective vibrational density of states $g(\omega)$ (weighted by the atomic cross section). In the one-phonon approximation, we have

$$S_{inc}(Q, \omega) = \frac{3N\hbar}{2M} e^{-2W} Q^2 \frac{n(\omega) + 1}{\omega} g(\omega) \quad (1)$$

with the Debye-Waller factor e^{-2W}, $W = \frac{1}{6} Q^2\langle u^2\rangle$, the mean squared displacement $\langle u^2\rangle$, the Bose occupation factor $n(\omega)$, the mass of the scatterer M, and the number of scattering atoms N (*8*).

Several categories of experiments have been undertaken to measure $S(Q, \omega)$ or its time Fourier-transform $S(Q, t)$.

1) Time of flight (TOF) experiments measure the flight time between the scattering event and the detection at a scattering angle 2Θ (cold neutrons, which are used here, have an inverse velocity $1/v_n$ on the order of 1×10^{-3} to 2×10^{-3} s/m). The TOF data are easily converted to $S(2\Theta, \omega)$ and can then be interpolated to $S(Q, \omega)$.

2) Backscattering experiments, which require a special type of triple axes spectrometer, define and analyze the neutron energy with perfect single-crystal monochromators in exact backscattering (thus, the Bragg angle $\vartheta = 90°$ to improve the energy resolution $\delta E/E \sim \cot\vartheta d\vartheta$) (*9*). Intensities are converted easily to $S(Q, \omega)$.

3) Neutron spin echo (NSE) experiments investigate the Larmor precessions of the neutron spin in a magnetic field to determine the neutron velocity change during the scattering event (*10*). The intermediate scattering function $S(Q, t)/S(Q, 0)$ is measured directly. More detailed information about neutron scattering may be found in (*8*).

Static Structure Factor

Let us start first with the structural information that can be deduced from neutron diffraction. The static structure factor $S(Q)$ can be regarded as a snapshot of the structure and can be measured up to high values of Q with good resolution in Q by neutron diffraction on deuterated polymers at short wavelengths. Figure 1A shows an example for deuterated polybutadiene (PB) (*11*), a main chain polymer without side groups. Measurements at three temperatures are compared: 4 K, T_g = 186 K, and 270 K. No qualitative changes are observed within this temperature range.

In fact, the main changes with temperature are a shift of the peak position of the first peak in $S(Q)$ (Fig. 1B) and a change of its width (Fig. 1C), which confirm that this peak is mainly the result of interchain contributions. The thermal change of the peak position, that is the thermal expansion between the polymer chains, is smaller in the glassy state than it is above T_g. This is known from macroscopic dilatometric experiments. If we assume that the peak width Γ of the first peak arises from a distribution of nearest neighbor distances with a correlation length $\zeta = 4\pi/\Gamma$, then we find that ζ increases with decreasing temperature down to somewhere below T_g and finally freezes at a value of ζ = 34 Å. Thus, we observe a tendency toward local ordering.

Side Group Motion in the Glass

Within the glassy state, trans-gauche isomerizations (rotations about single bonds of the main chain), which are involved in the diffusion of the polymer chain at high temperatures, are restricted, which is not the case for local motions like side group motions. Probably the most simple example of a side group motion is the rotation of a methyl group about its threefold axis. Inelastic neutron backscattering and TOF experiments with partially deuterated samples were used to investigate the dynamics of methyl groups in polyisoprene (PI) (*12*). The strictly elastic scattering, which can be measured with very high energy resolution (microelectron volts), is very sensitive to the slow molecular motion that gives rise to a broadening of the elastic line; this process is also called quasi-elastic scattering. When the time scale of motion becomes comparable with the corresponding energy resolution, the measured intensity in the elastic window drops (Fig. 2). The elastic intensity I_{el} decreases with temperature as well because of the Debye-Waller factor. For an unlabeled (protonated) sample, the inelastic scattering is dominated by incoherent scattering from the hydrogen atoms. In the case presented here, the backbone (PI-d5) enhances the contrast with respect to fully deuterated PI-d8 or PI-d3. Thus, the relative contribution of the methyl group with respect to the total scattering of the monomer gets strongly enhanced if the backbone is deuterated (PI-d5), and it is much weaker for deuterated methyl groups (PI-d3, PI-d8).

In Fig. 2, we show the elastic scattering of PI as a function of temperature, normalized to T = 1.5 K, at which temperature all molecular motions should be frozen. The elastic intensity decays in two steps for the samples with protonated methyl groups and in one step for samples with deuterated methyl groups. The first low-temperature step of the elastic scattering indicates that the relaxation times for methyl group rotation enter the dynamical window of the spectrometer. With increasing temperature, the relaxation times get shorter and the corresponding quasi-elastic scattering is broad. The elastic scattering levels off near T = 160 K (below T_g). From model calculations, we conclude that the observed, relatively slow intensity decay can be ascribed to a wide distribution of activation energies or relaxation times (*12*) that results from the local disorder. The second step observed for the elastic scattering at all degrees of deuteration is a signature of the glass transition.

In the far inelastic range, we make use of TOF measurements to observe the librational mode of the methyl group located at ~23 meV (Fig. 3). Again, isotope substitution can be used efficiently to determine the

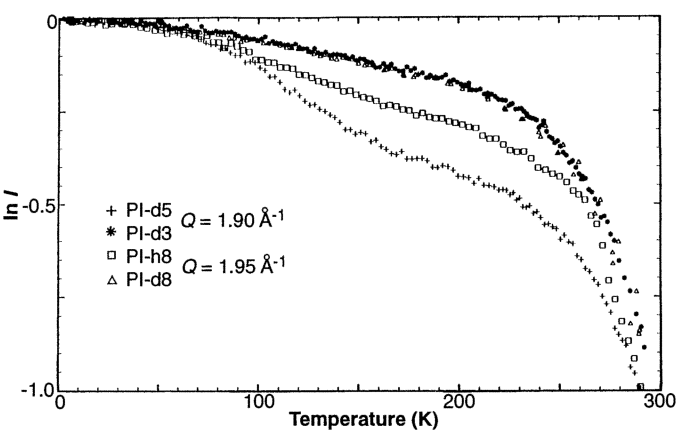

Fig. 2. Elastic scattering of PI for different degrees of deuteration. The intensity decrease shows the onset of the dynamics on a time scale faster than picoseconds (*12*); the first step in the temperature dependence arises from the methyl-group dynamics, the second step from the glass transition. All samples have microstructures with about 93% 1,4-PI and 7% 3,4-PI (*12*). Intensity is normalized to the value at T = 1.5 K.

origin of the observed mode because for deuterated side groups the librational mode weakens and shifts toward lower frequencies. In our example, the mode must be hidden under the stronger vibrational scattering of the protonated polymer backbone.

The Boson Peak

We have seen that in the glassy state, local motions are possible. A different type of libration, that of the polymer backbone, appears at much lower frequencies because it involves several heavy atoms. In a crystal, these vibrations would be propagating torsional modes.

At low frequency, the Debye vibrational density of states reveals itself in the incoherent scattering $S_{inc}(Q, \omega)$ as a constant contribution [because $g_{Debye}(\omega) \approx \omega^2$, and at low frequency, $n(\omega) \approx k_B T/\omega$; therefore, from Eq. 1, $S_{inc}(Q, \omega) \sim$ constant] and can be estimated from the sound velocity. A characteristic feature of glasses (ionic, inorganic, low molecular weight network, or polymer glasses) is that one observes between 0.1 and 5 meV a pronounced excess intensity over the estimated Debye level. This is found in neutron and Raman spectra as an inelastic peak in $S(Q, \omega)$ called the "boson peak." Neutrons have the advantage that the vibrational density of states can be measured directly, whereas for light scattering, a coupling constant $c(\omega)$ enters that itself depends on frequency in an unknown fashion (*13*).

The existence of the boson peak is most probably related to the well-known low-temperature anomalies of the specific heat and the thermal conduction of glasses. One can deduce this from a comparison of the measured specific heat with the specific heat calculated from neutron or Raman spectra. The origin of the boson peak, however, is not well understood, and it is currently the subject of both experimental and theoretical efforts.

We compared the boson peak for different polymers, including a highly crystalline polymer, *trans*-1,4-polybutadiene (*trans*-PB-h6), (Fig. 4), at temperatures well below T_g. Whereas the inelastic scattering for the crystalline polymer is flat in the low-frequency region, the boson peak shows up for all other glassy polymers. It is located at frequencies of ~1 meV for the very flexible polydimethylsiloxane (PDMS) and at ~2.3 meV for the sterically hindered polyisobutylene (PIB) (*14*). Recently, a connection between the fragility of glass formers and the boson peak was proposed (*13*). A collection of our data suggests that there is a correlation between the mobility of the polymers above T_g (that is, the monomeric friction coefficient) and the boson peak. Polymer glasses that have a high flexibility above T_g, such as PDMS, exhibit excess vibrations or librations at lower frequency and with greater amplitude, whereas the boson peak of sterically hindered polymers, such as PIB, is found at higher frequency. Although this does not explain the origin of the boson peak, it might indicate that a nonequilibrium state is formed above T_g dependent on the local mobility of the chain.

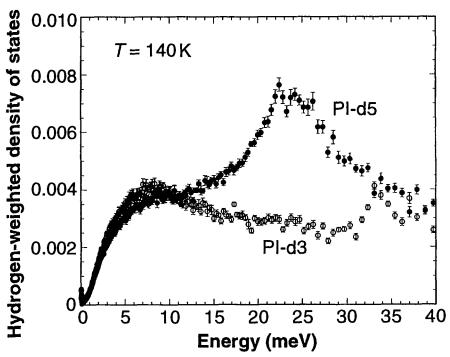

Fig. 3. Methyl group librational mode of side group deuterated (d3) and main chain–deuterated (d5) PI (*12*).

Fast Process near T_g

Changes appear in the neutron spectra as the temperature is increased near T_g. At first glance, we would not expect changes of the dynamics in the picosecond range of neutron scattering experiments because the structural relaxation times diverge with a Vogel-Fulcher law and become extremely long. Nevertheless, the local dynamics for times shorter than picoseconds change at temperatures near T_g, as can be seen from both the elastic scattering and the inelastic low-frequency scattering.

The elastic scattering, for example, for PI (Fig. 2), drops strongly near the glass transition. This effect is not caused by any side-group dynamics and is observed for polymers that have no side groups, like PB (*15*), and for low molecular weight glasses (*16*, *17*). From the Q-dependence of the elastic scattering I_{el} ($I_{el} = I_0 e^{-2W}$, where I_0 is a constant), we can deduce the effective mean squared displacement $\langle u^2 \rangle$. The temperature dependence of $\langle u^2 \rangle$ at very low temperatures is almost linear, as expected for harmonic vibrations. However, with increasing temperature, we see an upturn of $\langle u^2 \rangle$ that becomes very pronounced near T_g. Here we chose PB as an example (*15*) (Fig. 5), but the same effect is observed for other polymers [such as PIB (*18*) or PI (*12*)].

In the temperature range where $\langle u^2 \rangle$ increases strongly (Fig. 5), backscattering experiments at high energy resolution still indicate a purely elastic component, that is, the observed decrease of the elastic scattering does not arise from a broadening of the elastic line. However, in the inelastic range, we observe a change of the low-frequency scattering (Fig. 6). Within the glassy state and at higher frequencies, it is possible to account for the increase in inelastic intensity with temperature through the Bose oc-

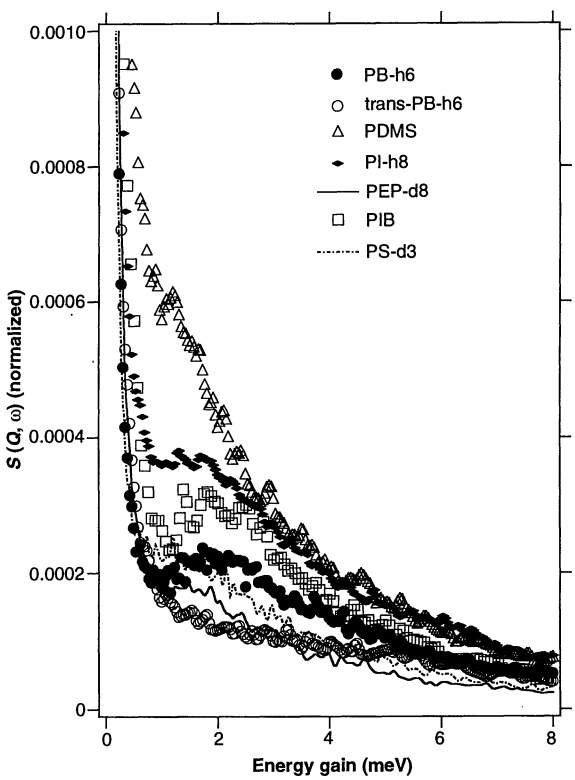

Fig. 4. Low-temperature spectra of various amorphous polymers with different microstructure (T = 100 K) showing the boson peak as compared to the crystalline *trans*-PB-h6. Abbreviations: PB-h6, protonated polybutadiene; PDMS, protonated polydimethylsiloxane; PI-h8, protonated polyisoprene; PEP-d8, fully deuterated polyethylenepropylene; PIB, fully protonated polyisobutylene; PS-d3, main chain–deuterated polystyrene. The boson peak moves toward lower energy for increasing melt mobility (*30*). The spectra are interpolated to constant Q = 1.4 Å^{-1} and are normalized to the integral scattering in the energy range −2 to 8 meV.

cupation factor, as expected for harmonic vibrations. At higher temperatures, however, the increase of the inelastic scattering at frequencies below the boson peak varies more strongly than with the Bose factor (Fig. 6). In the same temperature range, the first peak of the static structure factor $S(Q)$ (Fig. 1) of PB shows a change in line width and peak position. The width of the observed low-frequency excess scattering does not depend on temperature and the momentum transfer Q, but its intensity increases with Q^2 for incoherent and with $S(Q)\,Q^2$ for coherent scattering samples. This dependence on Q is found for the boson peak as well, suggesting a common origin. For PB, the observed low-frequency scattering seems to be centered around an energy $E \approx 0$ meV, that is, it is quasi-elastic, as is seen for many fragile glass formers. However, the study of the less fragile PIB has revealed that this fast process can be clearly inelastic (*14*).

Slow Relaxation Above T_g

Whereas the fast process occurs on a time scale of picoseconds, a slower process is observed above T_g. We have studied this process on deuterated polybutadiene and polyisoprene samples using NSE techniques. This method gives excellent energy resolution over a relatively wide dynamic range. The normalized intermediate scattering function $S(Q, t)/S(Q, 0)$ is measured directly by this technique.

The intermediate scattering function for deuterated PB-d6 is presented in Fig. 7A at the peak of the static structure factor (Q = 1.4 Å^{-1}). With increasing temperature, the relaxation becomes faster and the α-relaxation is then observed as a decay of the experimental curves inside the time window of the instrument. We observe the fast relaxation process indirectly as a missing fraction, which results in $S(Q, t)/S(Q, 0) < 1$ for $t \to 0$. The temperature dependence of the decrease of this constant is shown in the inset of Fig. 7B.

To demonstrate this effect, we rescale the time axis of the observed relaxation curves with the time-temperature superposition principle so that they follow the time scale of the viscosity relaxation. The viscosity η of polymers can be related to the monomeric friction coefficient ζ by $\eta = \zeta/k_BT$, where $\zeta(T)$ follows the Vogel-Fulcher-Tamman temperature dependence: $\zeta = \zeta_0\exp[1/\alpha(T - T_0)]$, with T_0 = 128 K, $\alpha = 7.12 \times 10^{-4}$ K^{-1}, and $\zeta_0 = 1.26 \times 10^{-11}$ dyne s cm^{-1} (*19*). We assume that the relevant relaxation time on the microscope level is given by $\tau(Q) = \tau_0\zeta(T)/T$, and thus, we fit τ_0 as the only parameter common to all temperatures and scale the observation time by t/τ. This procedure leads to a good master plot of the microscopic data merely by applying the temperature dependence of the macroscopically observed relaxation time (Fig. 7B). Thus, we conclude that the same temperature dependence governs the dynamics of the macroscopic and microscopic quantities and that the time-temperature superposition principle is valid even on the microscopic time scale. This by no means trivial observation was first made for the ionic glass former $Ca_{0.6}K_{0.4}(NO_3)_{1.4}$ (*20*).

The shape of the relaxation function in Fig. 7B is not a simple exponential but

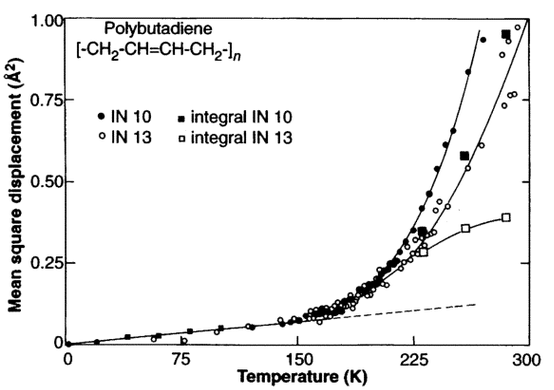

Fig. 5. Mean squared displacement for PB as deduced from the Q-dependence of elastic scattering data (*15*) and measured on the neutron backscattering instruments IN10 (1-μeV energy resolution) and IN13 (8-μeV energy resolution).

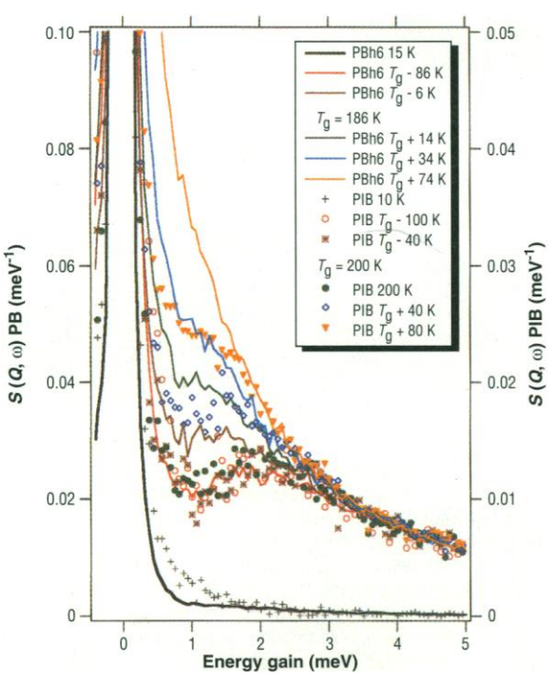

Fig. 6. The scattering function $S(Q, \omega)$ for PIB at Q = 1.4 Å^{-1} (markers) and PB (lines) and resolution functions (lower curve). The curves are corrected for the Bose temperature factor and scaled to their glass transition temperature. An increase in intensity caused by harmonic vibrations results in a common curve. Near the glass transition temperature, additional low-frequency scattering appears, which seems usually to be quasi-elastic but can be clearly inelastic, as shown for PIB (the PIB curves are scaled by a common factor to have the same intensity as for PB at 4 to 5 meV).

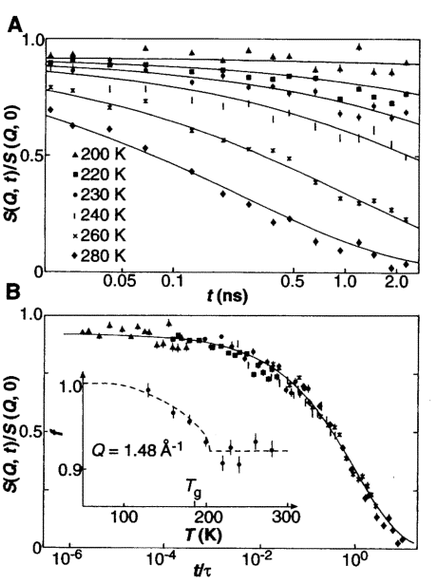

Fig. 7. The α-relaxation process at the main peak of $S(Q)$ for PB (*31*) (**A**) as measured by NSE at several temperatures, and (**B**) rescaled by a characteristic relaxation time as deduced from viscosity data. (**Inset**) Temperature dependence of the fraction f that relaxes by a process faster than the α-relaxation. The fraction that relaxes by means of the α-relaxation is represented by the nearly constant part of the curve.

follows a so-called stretched exponential or the Kohlrausch-Williams-Watts (KWW) function: $S(Q, t)/S(Q,0) = f^0(Q) \exp[-(t/\tau)^\beta]$ where $\beta = 0.45$ at $Q = 1.48$ Å^{-1} or even less at a higher value of Q ($\beta = 0.38$ at $Q = 1.88$ Å^{-1}). The lines in Fig. 7A are fit curves to the KWW function at $Q = 1.48$ Å^{-1}. The fitted prefactor $f^0(Q)$ shows nearly no change with temperature above about $T_c = T_g + 30$ K (Fig. 7B, inset), but below T_c, the total observed amplitude increases as described above. This is more clearly seen at a higher value of Q and was interpreted as the predicted square root singularity from MCT (*21*).

An interesting observation is also made for the Q-dependence of the prefactor $f^0(Q)$ of the KWW function, that is, the fraction that relaxes through the α-relaxation, and for the relaxation rate. As shown in Fig. 8, $f^0(Q)$ has a maximum at the main peak position of the static structure factor. The Q-value of the peak position corresponds to distances that are preferred by the system, and therefore, it is plausible that the relaxation rate is minimal at this value of Q, in agreement with the so-called de Gennes narrowing (*22*) and predictions of the MCT (*4*).

Whereas the above results for the α-relaxation are in agreement with MCT, we add a result for $S(Q, t)/S(Q, 0)$ at $Q = 1.88$ Å^{-1}, the minimum after the structure factor peak, which disagrees with idealized version of the MCT. Measurements at higher values of Q show that the construction of the master function, analogous to Fig. 7, is possible only above $T_c = T_g + 30$ K. At a temperature of about 215 K, deviations from this scaling appear. We present the relaxation rates at $Q = 1.88$ Å^{-1} for different temperatures as an Arrhenius plot (Fig. 9) (*23*) and find, for temperatures above T_c, a Vogel-Fulcher curve for the measured relaxation rates, analogous to the viscosity relaxation. For $T < T_c$, the microscopic time scale, as observed by neutron scattering, bifurcates from the viscosity time scale at about 10^8 Hz and shows an Arrhenius behavior. Such a scenario is similar to the splitting of the β-relaxation from the α-relaxation, as known from studies such as dielectric experiments (*5*, *24*). A direct comparison with dielectric data has recently been performed (*25*) and has shown that there exists a third dynamical process, the slow β-process. In other words, the fast β-process, which has commonly been associated with MCT, is distinctly different from the slow β-relaxation observed by dielectric spectroscopy.

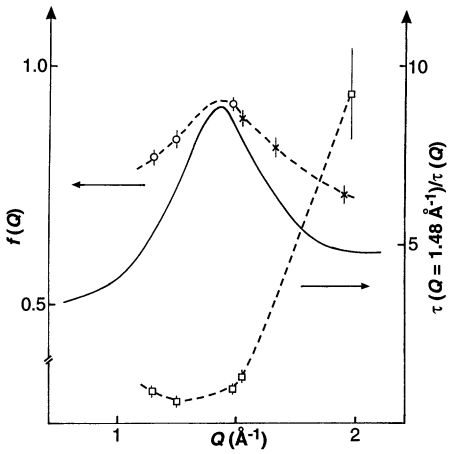

Fig. 8. The Q-dependence of the α-relaxation strength (dotted line, left axis) compared with the static structure factor (solid line) and ratio of α-relaxation rate $\tau(Q = 1.48$ Å$^{-1})/\tau(Q)$ (dotted line, right axis) (*31*).

Conclusions

The neutron scattering experiments presented above explore the structure and the microscopic dynamics of polymers in the glass and in the melt close to T_g. The structure does change marginally passing from the glass to the melt. The thermal expansion affects the position and width of the first diffraction peak, an indication for minor changes in the medium-range order. In the same temperature region, the dynamic scattering function starts to convert with increasing temperature from an inelastic spectrum (boson peak) toward a quasi-elastic spectrum. The scattering in the low-temperature range is describable by a harmonic behavior. At higher temperatures, a stronger temperature dependence is observed for both the low-frequency scattering and the mean squared displacement with respect to the low-temperature harmonic behavior. In most cases, the fast dynamic process that appears close to T_g seems to be centered around $E \approx 0$. This behavior is different for less fragile glasses like PIB (*14*). For these systems, the temperature-dependent scenario near T_g is similar, but the fast dynamic process is inelastic (up to about $T_g + 40$ K for PI). This difference raises the question of a possible connection between the fast dynamic process and vibrational features that relate to the boson peak. In terms of the soft-potential model, such a connection has recently been made where the low-frequency vibrations and relaxations were derived from the same soft potential (*26*). The soft-potential model is an extension of the phenomenological two-level model invoked for the description of the low-temperature tunneling states in glasses. According to this model, a large part of the fast dynamical process would be of vibrational origin. The situation is much more clear for the slowest process, the α-relaxation, which we observe as a stretched exponential decay by NSE. From the highest investigated temperatures down to about $T_g + 35$ K, the temperature dependence follows the time scale of the viscosity relaxation, which identifies it clearly as the α-process. Below that temperature, NSE most likely observes the Johari-Goldstein β-relaxation, which appears to be distinctly different to the fast process.

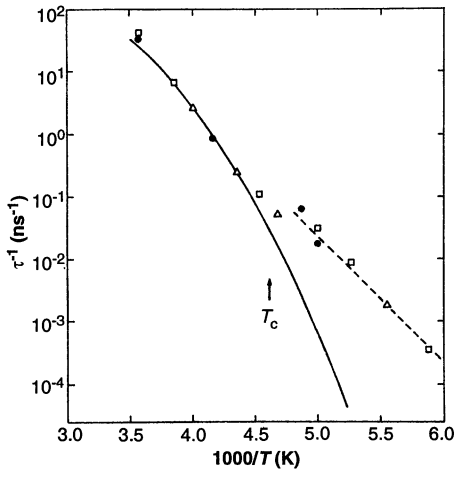

Fig. 9. The Arrhenius plot of the α-relaxation rate at $Q = 1.88$ Å^{-1} obtained from Kohlrausch fits to the NSE data. The solid line presents the temperature behavior of the time scale as deduced from the monomeric friction coefficient, which follows a Vogel-Fulcher behavior. The dashed line shows that the observed relaxation times below T_c follow an Arrhenius behavior as known for the "classical" β-relaxation (*23*), confirmed by recent dielectric experiments (*25*).

One of the great advantages of neutron scattering is the weak interaction with material, which nevertheless yields low scattering intensities. The investigation of the glass transition affords a wide dynamic window. For neutron scattering, there is no problem on the short time side. Toward longer times, the instrumental resolution has to be improved, as it is currently done by new neutron backscattering and spin echo spectrometers. To understand the physics of the glass transition, where relaxation rates change by more than 12 decades, we inevitably need a combination of complementary experimental techniques. Light scattering has proved to be a very efficient tool in the investigation of the glass transition, and neutron scattering might help clarify the frequency-dependent light coupling constant. The high-frequency motions that are explored by neutron scattering often influence the spectra of NMR and dielectric experiments, but neutrons do not reach this low-frequency regime. Again, a combination of these techniques is very desirable [see, for examples, (*24*, *27*, *28*)]. Computer simulations, which are being applied to more and more realistic polymer glasses and melts, can access the same time range as neutron scattering and thus allow a direct comparison of model and reality. Thus, the microscopic understanding of

polymers, to which neutron scattering contributes, might have an impact on the development of new materials in the future.

REFERENCES AND NOTES

1. J. D. Ferry, *Viscoelastic Properties of Polymers* (Wiley, New York, 1980).
2. W. Kauzmann, *Chem. Rev.* **43**, 219 (1948).
3. See, for example, J. Jäckle, *Rep. Prog. Phys.* **49**, 171 (1986).
4. W. Götze, *Liquids, Freezing and the Glass Transition*, J. P. Hansen, D. Levesque, J. Zinn-Justin, Eds. (North-Holland, Amsterdam, 1991), p. 287.
5. G. P. Johari and M. Goldstein, *J. Chem. Phys.* **53**, 2372 (1970).
6. See, for example, R. G. Kirste, W. A. Kruse, J. Schelten, *Makromol. Chem.* **162**, 299 (1973).
7. "Incoherent" stands for spin incoherent nuclear scattering; see, for example, (*8*).
8. S. W. Lovesey, *Theory of Neutron Scattering from Condensed Matter*, vol. 1 of *The International Series of Monographs on Physics* (Clarendon, Oxford, 1984).
9. B. Alefeld, *Bayer. Akad. Wiss. Math. Naturwiss. Kl.* **11**, 109 (1966).
10. F. Mezei, *Neutron Spin Echo* (Springer-Verlag, Berlin, 1980).
11. B. Frick, *Prog. Colloid Polym. Sci.* **80**, 164 (1989).
12. _____ and L. J. Fetters, *Macromolecules* **27**, 974 (1994).
13. See, for example, A. P. Sokolov, A. Kisliuk, D. Quitmann, E. Duval, *Phys. Rev. B* **48**, 7692 (1993).
14. B. Frick and D. Richter, *ibid.* **47**, 14795 (1993).
15. _____, W. Petry, U. Buchenau, *Z. Phys. B* **70**, 73 (1988).
16. A. J. Dianoux, W. Petry, D. Richter, Eds., "Dynamics of Disordered Materials II," *Physica A* **201**, 1 (1993).
17. D. Richter, A. J. Dianoux, W. Petry, J. Teixeira, Eds., *Dynamics of Disordered Materials* (Springer-Verlag, Berlin, 1989), vol. 37.
18. B. Frick, D. Richter, S. Treviño, *Physica A* **201**, 88 (1993).
19. G. C. Berry and T. G. Fox, *Adv. Polym. Sci.* **5**, 261 (1968).
20. F. Mezei, W. Knaak, B. Farago, *Phys. Rev. Lett.* **58**, 571 (1987).
21. B. Frick, B. Farago, D. Richter, *ibid.* **64**, 2921 (1990).
22. P. G. De Gennes, *Physica* **25**, 825 (1959).
23. D. Richter, R. Zorn, B. Farago, B. Frick, L. J. Fetters, *Phys. Rev. Lett.* **68**, 71 (1992); see also E. Rößler, *ibid.* **69**, 1620 (1992); D. Richter, R. Zorn, B. Farago, B. Frick, L. J. Fetters, *ibid.*, p. 1621.
24. E. Rössler, A. P. Sokolov, P. Eiermann, U. Warschewske, *Physica A* **201**, 273 (1993); *ibid.*, p. 256.
25. R. Zorn and F. I. Mopsik, unpublished results.
26. U. Buchenau, *Europhys. News* **24**, 77 (1993); U. Buchenau *et al.*, *Phys. Rev. Lett.* **73**, 2344 (1994).
27. J. Colmenero, A. Alegria, J. M. Alberdi, F. Alvarez, B. Frick, *Phys. Rev. B* **44**, 7321 (1991); J. Colmenero, A. Arbe, A. Alegria, *Phys. Rev. Lett.* **71**, 2603 (1993).
28. R. Zorn *et al.*, *Physica B* **180–181**, 534 (1992).
29. B. Frick, D. Richter, C. Ritter, *Europhys. Lett.* **9**, 557 (1989).
30. B. Frick and D. Richter, unpublished results.
31. D. Richter, B. Frick, B. Farago, *Phys. Rev. Lett.* **61**, 2465 (1988).

32. We gratefully acknowledge the fruitful collaboration with U. Buchenau, R. Zorn, and B. Farago in much of the presented work and the excellent sample preparation by L. J. Fetters.

Physical Aging in Polymer Glasses

Ian M. Hodge

Physical aging refers to structural relaxation of the glassy state toward the metastable equilibrium amorphous state, and it is accompanied by changes in almost all physical properties. These changes, which must be taken into account in the design, manufacture, and use of glassy polymer materials and devices, present a daunting challenge to theorists.

Glasses usually exist in a nonequilibrium state, and relaxation toward equilibrium is commonly referred to as physical aging. This term was first coined by Struik (*1*) to distinguish glassy state relaxation from other time-dependent processes such as recrystallization and chemical degradation. In the inorganic glass literature, it is traditionally referred to as structural relaxation, annealing, or stabilization. The variety of terminologies reflects the common occurrence and considerable practical importance of glassy state relaxation to a chemically diverse range of materials that includes polymers, inorganic glasses, composites, amorphous metals, and even foodstuffs. Physical aging is particularly important for polymers, because the rate of physical aging is determined in part by how far below the glass transition temperature T_g the polymer is used, and T_g values are lower for polymers than for most inorganic glasses. Physical aging also affects the characteristic time scale of dynamic properties, which are important for polymers. The coupling between thermodynamic and dynamic properties gives rise to the most practically important and technically difficult aspect of physical aging, its nonlinearity. Accurate prediction of changes in physical properties with aging can have significant economic implications, in part because of the obvious need to predict long-term behavior from accelerated short time tests. These and other issues are discussed in detail in several recent review articles and books (*1–5*), a report of a recent workshop at the National Institute of Standards and Technology (NIST) (*6*), and in the proceedings of two international conferences (*7*, *8*). Properties and applications affected by physical aging include the design, manufacture, and performance of polymer-based composites, automotive applications of polymers, adhesives, permeability of packaging materials, curling of photographic film supports, nonlinear optic materials, curing of epoxies, the optical, electrical, and mechanical properties of xerographic materials, and glass-to-metal seals.

In addition to being nonlinear, glassy state relaxations are also nonexponential and exhibit the memory effect, that is, relaxation from a particular state depends not only on what that state is, but also on how that state was reached. For example, physical aging of a polymer that has been injection molded will depend on the temperature T, hydrostatic pressure, and mechanical deformation history during the molding process, as well as the post-molding thermal and mechanical history before the polymer is put into service. The two essential ingredients of nonlinearity and nonexponentiality are illustrated by the effects of physical aging on viscoelastic creep shown in Fig. 1. The tensile creep compliance of poly(vinyl-chloride) (PVC) is shown as a function of creep time, measured after the indicated physical aging times, t_a, at 20°C after a quench from above T_g. The creep curves continue to move to longer creep times, even after almost 3 years of aging. The shapes of the individual curves are determined by the nonexponential compliance response function, which depends on material type, but is almost independent of t_a for these particular data. The latter independence allows a master creep compliance curve to be constructed by shifting the individual curves along the creep time axis (*9*), exemplified by the master curve at t_a = 1000 days. This procedure is not always possible for all properties and all polymers, however, because the response function often changes with annealing time. The effects of physical aging are erased by heating the glass above its T_g, indicating a close connection between aging and the glass transition. This effect is illustrated by the crossed data in Fig. 1, observed for a previously aged sample that had been heated to above T_g and aged again for 1 day, which essentially superimposed those of the original material after a day of aging.

The position of a curve on the creep time axis is determined by the average creep relaxation time, τ (*10*). Shifts along the creep time axis with aging can therefore be described in terms of τ increasing with aging time, t_a, approximated as:

$$\tau = \tau_0 t_a^{\mu} \qquad (1)$$

where μ is the Struik shift factor (*1*). Viscoelastic creep occurs because there is appreciable polymer chain mobility in the glassy state, and this mobility is determined by the free volume, v_f, and configurational entropy,

The author is at Eastman Kodak Company, Imaging Research and Advanced Development, Rochester, NY 14650–2116, USA.